Fabrication and characterization of fiber Bragg grating based sensors for force measurements

Marcos A. Kamizi, Marcelo A. Pedroso, José L. Fabris and Marcia Muller

Graduate Program in Electrical and Computer Engineering - CPGEI
Federal University of Technology - Paraná - UTFPR
Curitiba, Brazil
E-mail: marcoskamizi@gmail.com

Abstract— **This work describes a study about encapsulation of fiber Bragg gratings in elastomer materials for sensing purposes. Sensors were tested in measurements of forces resulting from loads applied to the sensor within a measuring interval from 0 to 1500 grams. It was analyzed the influence of the elastomer composition in the sensor response. Results point to the possibility of adjusting the responses in order to adequate the sensors for specific applications. Metrological characteristics were evaluated regarding the sensors sensitivity, linearity, hysteresis and resolution. The silicone elastomer DOW CORNING® BX3-8001 stood out due to the possibility of changing its hardness and also due to the lower cure time, resulting in a sensor with sensitivity of (0.312 ± 0.002) pm/g, resolution of (1.6 ± 0.6) g, linearity of ± 4.19 % and hysteresis of ± 6.29 %.**

Keywords—FBG encapsulation, FBG sensor, Polydimethylsiloxane, Silicone, elastomer material.

I. INTRODUCTION

In a few cases, the transducer encapsulation may be the way to make viable the sensing process. In this sense, the encapsulation must be designed to fulfill the project requirements. Examples may include the amplification or attenuation of some physical effect, the increase in the mechanical strength of the device or even the transducer housing. Generally speaking, encapsulation allows transforming a constrained device (e.g. with a too small size) in a practical device. In electronics, involucra allowed the development of several components as transistors and integrated circuits. Even in this well developed area there is still research seeking for new types of encapsulation to make possible more demanding applications. An outstanding example is the effort for the development of flexible semiconductors. In this regard, the field of biomedical engineering shows a significant demand for new technologies where adaptability to complex curved surfaces - like the human body - is essential. Within this context, the development of new encapsulation methods for the production of flexible devices which can be installed in irregular surfaces or joints is fundamental [1-2].

A similar situation occurs in the field of instrumentation where flexible sensors encapsulated in silicone can be used to measure a variety of parameters like curvature, flexure and pressure among others, with the encapsulation representing a fundamental stage of the process. Characteristics as low weight and size, robustness and low energy consumption can also make the devices appropriate for a number of applications [3].

However, the inclusion of new elements to the set modifies the system response, with resulting effects that may be whether beneficial or not.

An increasing amount of applications using fiber Bragg gratings (FBGs) as sensors have been reported in the literature [4]. Nevertheless, mainly owing to their reduced size and fragility, encapsulation is mandatory to provide protection against agents in the external environment. FBG protection is just one of the reasons for the use of an adequate encapsulation: beyond the safety, the improvement of sensing performance must be considered. As an example, it can be mentioned the change in the mechanical strength and flexibility, allowing an expansion in the measuring interval or the achievement of a better resolution. Such factors justify the study of materials, shapes and techniques for the FBG encapsulation [5-7]. In this context, the development of transducers and sensors oriented for force and pressure measurement in biomedical engineering is a prospective area [8-9].

This work describes the project, production and characterization of FBGs encapsulated in different kinds of elastomers for force sensing applications. These sensors have a unique encapsulation shape differing only in the material employed for the involucrum. The process of cure and the difficulties for the production were qualitatively assessed. Sensitivity, linearity, resolution and hysteresis of the sensors were experimentally determined under conditions of repeatability and intermediate precision. In the characterization stage, Bragg wavelength shifts were measured as a result of forces produced by loads from 0 to 1500 g placed on the sensor surface in steps of 150 g.

II. METHODOLOGY

A. Sensor Fabrication

FBGs recorded in standard single mode optical fiber (SSMF, G-652 from Draktel) without previous hydrogenation are the basis for the sensors. Gratings were fabricated at the Photorefractive Devices Unit of the Federal University of Technology – PR (UTFPR) by the direct illumination of a phase mask with an excimer KrF laser (Coherent, Xantos XS), operating at 248 nm. All FBGs have reflectivity lower than 15%, bandwidth of (0.21 ± 0.12) nm, thermal sensitivity of (9.80 ± 0.05) pm/°C and strain sensitivity of (1.13 ± 0.05) pm/µε.

The materials used for housing the FBG sensors were: Room temperature vulcanization silicone cured with acetic acid (RTV-1) which is a transparent silicone elastomer based on dimethylsiloxane (Silicone from Selabond); Thermoplastic Adhesive (TA) composed of elastomers, silane and hydrocarbon resins (Adesivo selante from Selabond); Room Temperature Vulcanization silicone cured with a catalyst (RTV-2) (BX3-8001 from Dow Corning™).

Sensors were produced using a MDF (Medium-density fiberboard) mold with dimensions of 18 x 20 x 0.9 mm fabricated by CNC (Computer Numeric Control) machining. The resulting shape for the sensors was a disc with diameter D of 50 mm, flat base and convex upperpart with maximum height H of 8 mm as shown in Fig.1. Such shape was chosen foreseeing a future application of the sensor as insole in the biomedical field.
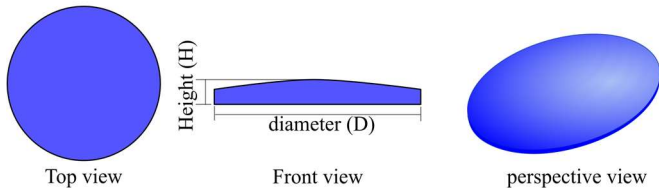

Fig. 1. Diagram representing the shape of the sensors.

RTV-2 was also used in a modified composition obtained with the controlled addition of quartz powder (SiO_2) to the commercial product. The hardness of the final product, room temperature vulcanization silicone plus quartz cured with a catalyst (RTV+Q), was analyzed.

The inclusion of quartz particles in the silicone elastomer causes a decrease in the elasticity of the final monomer owing to the strengthening of the chemical bonds between the polymer chains [10]. Quartz powder in the proportion of 50 % v/v were added to RTV-2 before the catalyst. No quartz was added to RTV-1 and TA elastomers owing to their high viscosity.

Before the sensor fabrication, it was applied on the mold a release agent (petroleum jelly based). Afterward, the FBGs were placed and fixed at the center of the diameter D of the mold, at half of its height H. Elastomers were previously prepared for application, according to manufacturer's instructions. The process was concluded by filling the mold with the elastomers. After the curing time (5 days for RTV-1 and TA, 24 hours for RTV-2 e RTV+Q) sensors were removed from the mold.

B. Characterization setup

Fig. 2 shows the schematic diagram of the interrogation system composed of a light source (Superlum LED Pilot-2, centered at 1558.2 nm with a FWHM of 73.8 nm) and an interrogation unit (IMON-512E, Ibsen Photonics, with 970 Hz maximum sampling rate, resolution < 0.5 pm). Reflection spectra of the FBGs under different loads were acquired and stored in a computer.
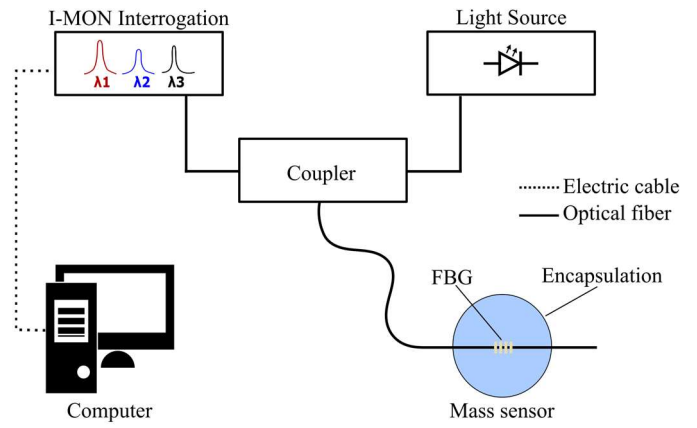

Fig. 2. Schematic diagram of the interrogation system.

Different loads were applied on the sensors by a material test machine composed of a compression equipment (z-stage), instrumented with a load cell with capacity up to 10 kg. Fig. 3 shows a picture of the experimental setup.
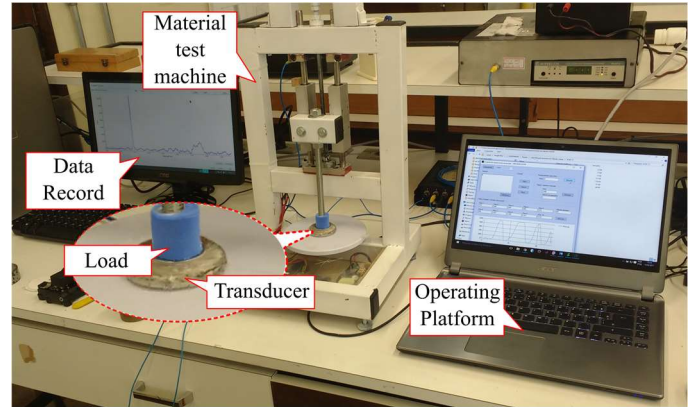

Fig. 3. Picture showing the experimental setup for the load application on the sensors.

The equipment was programmed to perform a routine for addition or subtraction of loads within the 0 – 1500 g measuring range in steps of 150 g. For each step, the load was kept constant and 5 measurements of the Bragg wavelength λ_B were acquired under repeatability condition. The up-and-down measuring cycle was repeated 3 times, resulting in 6 measurements under intermediate precision condition. The temperature was controlled during the experiment at (20 ± 0.5) °C.

C. Metrological Characteristics

The methodology for determining the metrological characteristics of the sensors was based on international standards for uncertainty analysis [11]. In this approach, the standard uncertainty associated to the *i-th* source of uncertainty is u_i for v_i degrees of freedom.

The main identified sources of uncertainty are: u_r (uncertainty under repeatability conditions of measurement), u_{ip} (uncertainty under intermediate precision conditions of measurement), u_{int} (resolution uncertainty of the interrogator), u_m (uncertainty of the material test machine) and u_t (uncertainty of the room temperature).

For Type A (statistical) uncertainties $u_i = \sigma_{mean}$, where $\sigma_{mean} = \sigma/\sqrt{n}$ is the experimental standard deviation of the mean for an experimental standard deviation σ obtained for n replicate measurements and $v_i = n - 1$ degrees of freedom. The resulting Type A standard uncertainties are $u_r = \sigma_{repeatability}$ and $u_{ip} = \sigma_{intermediate\_precision}$.

For Type B standard uncertainties (non-statistical) u_{int} , u_m e u_t are obtained by considering a $2a$-interval where the input measured quantity specified by the equipment manufacturer. In this case is assumed a symmetric rectangular distribution of probabilities for the measurand. The resulting standard uncertainty is then $u_i = a.3^{-1/2}$ with $v_i = \infty$ degrees of freedom.

Standard uncertainties measured in units other than picometers were transferred for the correct dimension by using an adequate coefficient of sensitivity s_i. The combined standard uncertainty u_c for 68.27 % confidence level is given by [12]:

$$u_c = \sqrt{\sum_{i=1}^{n}(s_i u_i)^2} \qquad (1)$$

Calibration curves were obtained by fitting linear functions to the experimental data by the method of least squares considering the combined standard uncertainties. In (2), λ_B is the resonance wavelength for an applied load m, λ_0 is the reference wavelength at null load ($m = 0$) and S_B is the sensor sensitivity (slope of the calibration curve), with a correlation coefficient r.

$$\lambda_B = \lambda_0 + m \qquad (2)$$

Resolution, linearity and hysteresis are obtained from the calibration curve. Resolution of the sensor is the ratio between the resolution of the interrogation unit (0.5 pm) and the sensitivity S_B (in pm/g). Linearity is the maximum absolute deviation of the experimental data points from the calibration curve. Hysteresis is the maximum value obtained by the arithmetic sum of absolute deviations of the experimental points from the calibration curve, relatively to a complete up-and-down cycle within the measuring interval.

The expanded uncertainty for a 95.45 % confidence level can be obtained according to (3), by multiplying the combined standard uncertainty by an appropriate coverage factor k_{veff}.

$$U^{95.45} = u_c . k_{v_{eff}}^{95.45} \qquad (3)$$

The coverage factor is based on a t-distribution for v_{eff} degrees of freedom given by (4).

$$V_{eff} = \frac{u_c^4}{\sum_{i=1}^{n} \frac{u_i^4}{v_i}} \qquad (4)$$

III. Results and Discussions

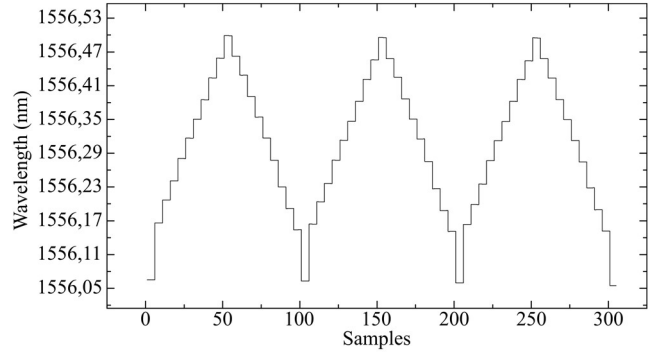Fig. 4 shows the responses of the RTV-1 sensor obtained in three up-and-down cycles.

Fig. 4. Response of sensor RTV-1 for three up-and-down cycles of measurement.

In each cycle, the first load increase from 0 to 150 g produces a wavelength shift significantly larger than those obtained with the subsequent load increments. This behavior indicates a diverse functional response for the RTV-1 sensor at this low-level load, related to a non-linearity in the response of the sensor for small loads. Owing to this non-linearity, the measuring range of the RTV-1 sensor was reset to 150 - 1500 g. A similar situation occurred for the sensor RTV+Q, however with a wider non-linear range when compared with the previous case. For the present case, it was possible do define two approximate linear measuring ranges: RTV+Q (0 - 600 g) and RTV+Q' (600 – 1500 g).

Fig. 5 and Fig. 6 show the calibration curves of all sensors. Each experimental point corresponds to the mean of the λ_B values obtained in different cycles for each applied load. Error bars stand for the combined standard uncertainties given by (1) considering the uncertainties $u_r, u_{ip}, u_{int}, u_m$ and u_t.
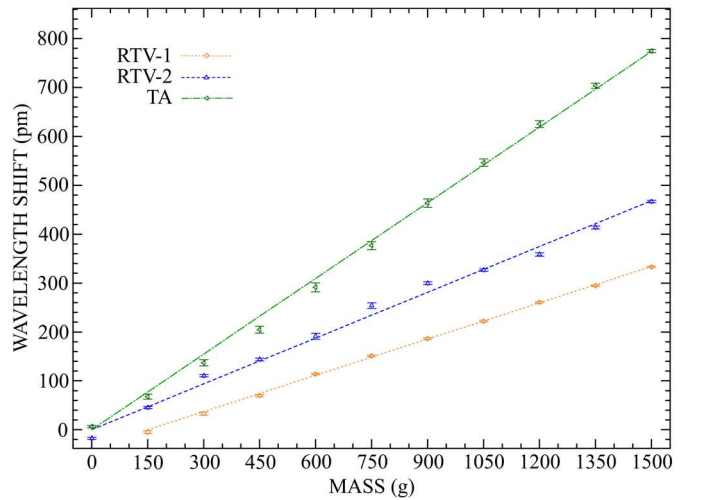

Fig. 5. Calibration curves of the RTV-1, RTV-2 e TA sensors. In a few cases the error bars are less than the symbol size.
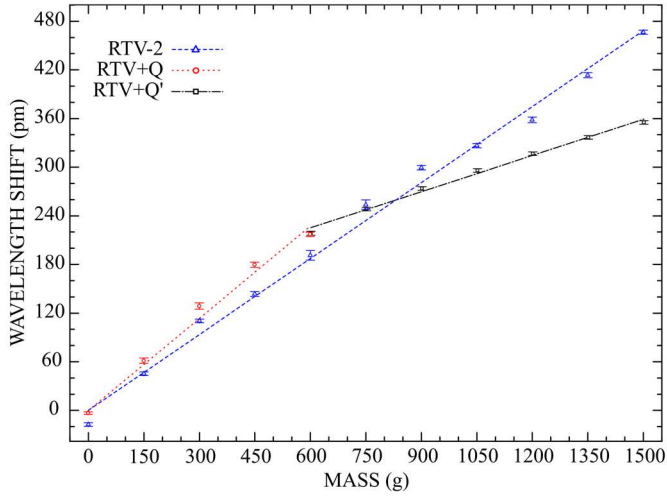
Fig. 6. Calibration curves of the RTV-2, RTV+Q e RTV+Q' sensors. In a few cases the error bars are less than the symbol size.

Metrological characteristics shown in Table I were determined considering the three up-and-down cycles. Linearity and hysteresis values, expressed in percent, were calculated with respect to the algebraic subtraction between the upper and lower limits (span) of the measuring interval.

Table I allows comparing the sensors and therefore, can be used in order to define which sensor will be used for an application with specific demands. All devices but RTV-1 present similar linearity and hysteresis, the performance of RTV-1 being superior regarding these characteristics (highlighted in green in Table I). Considering the resolution, sensor TA stands out (highlighted in blue in Table I).

The standard combined uncertainty u_c for 68.27 % confidence level, as well as the impact of each source of uncertainty on u_c are shown in Table II. The percentage values are taken relatively to u_c.

From data of Table II it becomes clear that, for all sensors but RTV-1, linearity and hysteresis (highlighted in red in Table II) are the most important sources of uncertainties contributing to the combined uncertainty. In the case of the RTV-1, its comparatively low linearity (highlighted in green in Table II) imparts precision to this device. Besides, measurements taken under conditions of intermediate precision are strongly impaired by the hysteresis. This is the major cause of dispersion in the measurements, increasing the combined uncertainty u_c.

TABLE II. Percentage of contribution of each standard uncertainty u_i to the standard combined uncertainty u_c.

Uncertainty	RTV-1	RTV-2	RTV+Q	RTV+Q'	TA
Repeatability (%)	0.01	0.01	< 0.01	< 0.01	< 0.01
Int. precision (%)	9.88	7.37	6.81	10.09	7.52
Linearity (%)	8.00	28.33	42.01	31.73	22.91
Hysteresis (%)	80.44	63.84	49.83	55.64	69.38
Resolution (%)	0.02	< 0.01	0.01	0.04	< 0.01
Mass (%)	0.69	0.23	0.83	0.52	0.10
Temperature (%)	0.96	0.21	0.52	1.98	0.09
u_c (g)	40.2	68.2	36.0	46.7	64.0

The expanded uncertainties for 95.45 % confidence level are shown in Table III. The degrees of freedom for u_r and u_{ip} are 4 and 5, respectively, and ∞ for the remaining uncertainties.

TABLE III. Expanded uncertainty for 95.45% confidence level.

	RTV-1	RTV-2	RTV+Q	RTV+Q'	TA
v_{eff}	225.15	223.64	198.91	86.94	257.67
$k_{v_{eff}}^{95.45}$	2.01	2.01	2.01	2.03	2.01
$U^{95.45}$ (g)	80.9	137.1	72.4	94.8	128.7

Regarding the fabrication, TA e RTV-1 elastomers do not require additives to activate their cure. Once exposed to room temperature, the cure sets up and a dry region develops from the rim toward the center of the involucrum. Also, these two elastomers have similar viscosities: among all tested materials, TA presents the higher viscosity, followed by the RTV-1. Unlike TA and RTV-1 elastomers, RTV-2 cure is activated by a catalyst. This silicone elastomer presents a change in the cure (hardening) after a few minutes, has the smallest viscosity among the all and the cure develops uniformly. The final shape of the sensor does not rely on injection molding. In this sense, the viscosity and cure process of the elastomers must be carefully considered in the sensor project. A smaller viscosity and a slow cure provide more time to stream the raw material into the mold, making easier the manufacture of the sensor.

TABLE I. Metrological characteristics of the sensors obtained under intermediate precision conditions.

Metrological characteristics	RTV-1	RTV-2	RTV+Q	RTV+Q'	TA
Measuring interval (g)	150-1500	0-1500	0-600	600-1500	0-1500
Reference wavelength (nm)	1556.164 ± 0.005	1533.299 ± 0.018	1533.409 ± 0.003	1533.633 ± 0.007	1529,578 ± 0.006
r coefficient	0.9997	0.9974	0,9966	0,9966	0,9996
Sensitivity (pm/g)	0.249 ± 0.002	0.312 ± 0.002	0.379 ± 0.005	0.149 ± 0.003	0.516 ± 0.002
Resolution (g)	2.0 ± 0.6	1.6 ± 0.5	1.3 ± 0.4	3.4 ± 1.0	1.0 ± 0.6
Linearity (%)	± 1.46	± 4.19	± 6.74	± 5.06	± 3.54
Hysteresis (%)	± 4.63	± 6.29	± 7.34	± 6.70	± 6.16

Such characteristics also result in a smooth surface of the sensor, improving the contact with the surface under sensing.

IV. CONCLUSION

We have shown a comparison of characteristics of force sensors based on FBG housed in different elastomer materials. These materials are suitable for FBG sensors as methods of fabrication are simple and do not demand the use of laboratory oven or vacuum camera. Besides, elastomer materials are resilient, flexible, low cost and easy to handle making the sensors not only cheap and durable but also versatile. The sensors of this work withstood to compressive stresses caused by applied loads from 0 g a 1500 g.

Mechanical deformations transferred to the FBG resulted in measurable wavelength shifts that allowed a complete characterization of the sensors. Linear responses to the applied loads were obtained for operation ranges that depend on the elastomer material. Sensitivity and operation range can be adjusted by an adequate choice of the elastomer material and fabrication parameters representing a fundamental step in the development of force sensors optimized for a specific application.

Among the tested materials, the RTV-2 stood out, as its mechanical characteristics may be changed by a controlled addition of quartz to the original formulation. RTV-2 was also the elastomer that resulted in a better quality for the sensor with the minor curing time and the easiest handling. However, comparing characteristics of linearity and hysteresis, RTV-2 produced a sensor with the worst performance ± 4.19 % for the linearity and ± 6.29 %. Among the sensors, the best values where obtained with the RTV-1 elastomer that resulted in a sensor with linearity of ± 1.46 % and hysteresis of ± 4.63 %.

REFERENCES

[1] D.-H. Kim, Z. Liu, Y.-S. Kim, J. Wu, J. Song, H.-S. Kim, Y. Huang, K.-c. Hwang, Y. Zhang, and J. A. Rogers, "Optimized structural designs for stretchable silicon integrated circuits," Small, vol. 5, no. 24, pp. 2841–2847, 2009.

[2] S. Wang, Y. Huang, and J. A. Rogers, "Mechanical designs for inorganic stretchable circuits in soft electronics," IEEE Transactions on Components, Packaging and Manufacturing Technology, vol. 5, no. 9, pp. 1201–1218, Sept 2015.

[3] G. Saggio, F. Riillo, L. Sbernini, and L. R. Quitadamo, "Resistive flex sensors: a survey," Smart Materials and Structures, vol. 25, no. 1, p. 013001, 2016.

[4] A. Cusano, A. Cutolo and J. Albert, "Fiber Bragg Grating Sensors: Research Advancements, Industrial applications and market exploitation," Bentham e Books, 2011.

[5] Liu, Q. Sheng, S. Muftu, A. Khademhosseini, M. L. Wang, and M. R. Dokmeci, "A stretchable and transparent swnt strain sensor encapsulated in thin pdms films," Transducers & Eurosensors XXVII: The 17th International Conference on Solid-State Sensors, Actuators and Microsystems (TRANSDUCERS & EUROSENSORS XXVII), pp. 1091–1094, June 2013.

[6] J. Nedoma, M. Fajkus, L. Bednarek, J. Frnda, J. Zavadil, and V. Vasinek, "Encapsulation of fbg sensor into the pdms and its effect on spectral and temperature characteristics," Advances in Electrical and Electronic Engineering, vol. 14, no. 4, 2016.

[7] M. Fajkus, J. Nedoma, R. Martinek, V. Vasinek, H. Nazeran, and P. Siska, "A non-invasive multichannel hybrid fiber-optic sensor system for vital sign monitoring," Sensors, vol. 17, no. 1, 2017.

[8] L. H. Negri, E. M. Schiefer, A. S. Paterno, M. Muller, and J. L. Fabris, "Smartphone-based portable intensity modulated force sensor," Proc. SPIE, vol. 9634, pp. 96 347S–96 347S–4, 2015.

[9] L. H. Negri, E. M. Schiefer, A. S. Paterno, M. Muller, and J. L. Fabriss, "An approach to improve the spatial resolution of a force mapping sensing system," Measurement Science and Technology, vol. 27, no. 2, p. 025103, 2016.

[10] M. Tsige, T. Soddemann, S. B. Rempe, G. S. Grest, J. D. Kress, M. O. Robbins, S. W. Sides, M. J. Stevens, and E. W. III, "Interactions and structure of poly(dimethylsiloxane) at silicon dioxide surfaces: Electronic structure and molecular dynamics studies," The Journal of Chemical Physics, vol. 118, no. 11, pp. 5132–5142, 2003.

[11] Evaluation of Measurement Data—Guide to the Expression of Uncertainty in Measurement 2008, JGCM 100:2008, published by BIPM in the name of BIPM, IEC, IFCC, ILAC, ISO, IUPAC, IUPAP and OIML.

[12] G. R. C. Possetti, R. C. Kamikawachi, M. Muller, and J. L. Fabris, "Metrological evaluation of optical fiber grating-based sensors: An approach towards the standardization," Journal of Lightwave Technology, vol. 30, no. 8, pp. 1042–1052, April 2012